



OPEN ACCESS

EDITED BY

Carine De Marcos Lousa,
Leeds Beckett University,
United Kingdom

REVIEWED BY

Shiyu Xia,
California Institute of Technology,
United States
Wojciech Kopec,
Max Planck Institute for Biophysical
Chemistry, Germany

*CORRESPONDENCE

Kristyna Pluhackova,
kristyna.pluhackova@simtech.uni-
stuttgart.de

SPECIALTY SECTION

This article was submitted to Membrane
Traffic,
a section of the journal
Frontiers in Cell and Developmental
Biology

RECEIVED 06 June 2022

ACCEPTED 26 July 2022

PUBLISHED 02 September 2022

CITATION

Korn V and Pluhackova K (2022), Not
sorcery after all: Roles of multiple
charged residues in membrane insertion
of gasdermin-A3.
Front. Cell Dev. Biol. 10:958957.
doi: 10.3389/fcell.2022.958957

COPYRIGHT

© 2022 Korn and Pluhackova. This is an
open-access article distributed under
the terms of the [Creative Commons
Attribution License \(CC BY\)](https://creativecommons.org/licenses/by/4.0/). The use,
distribution or reproduction in other
forums is permitted, provided the
original author(s) and the copyright
owner(s) are credited and that the
original publication in this journal is
cited, in accordance with accepted
academic practice. No use, distribution
or reproduction is permitted which does
not comply with these terms.

Not sorcery after all: Roles of multiple charged residues in membrane insertion of gasdermin-A3

Viktoria Korn and Kristyna Pluhackova*

Stuttgart Center for Simulation Science, Cluster of Excellence EXC 2075, University of Stuttgart, Stuttgart, Germany

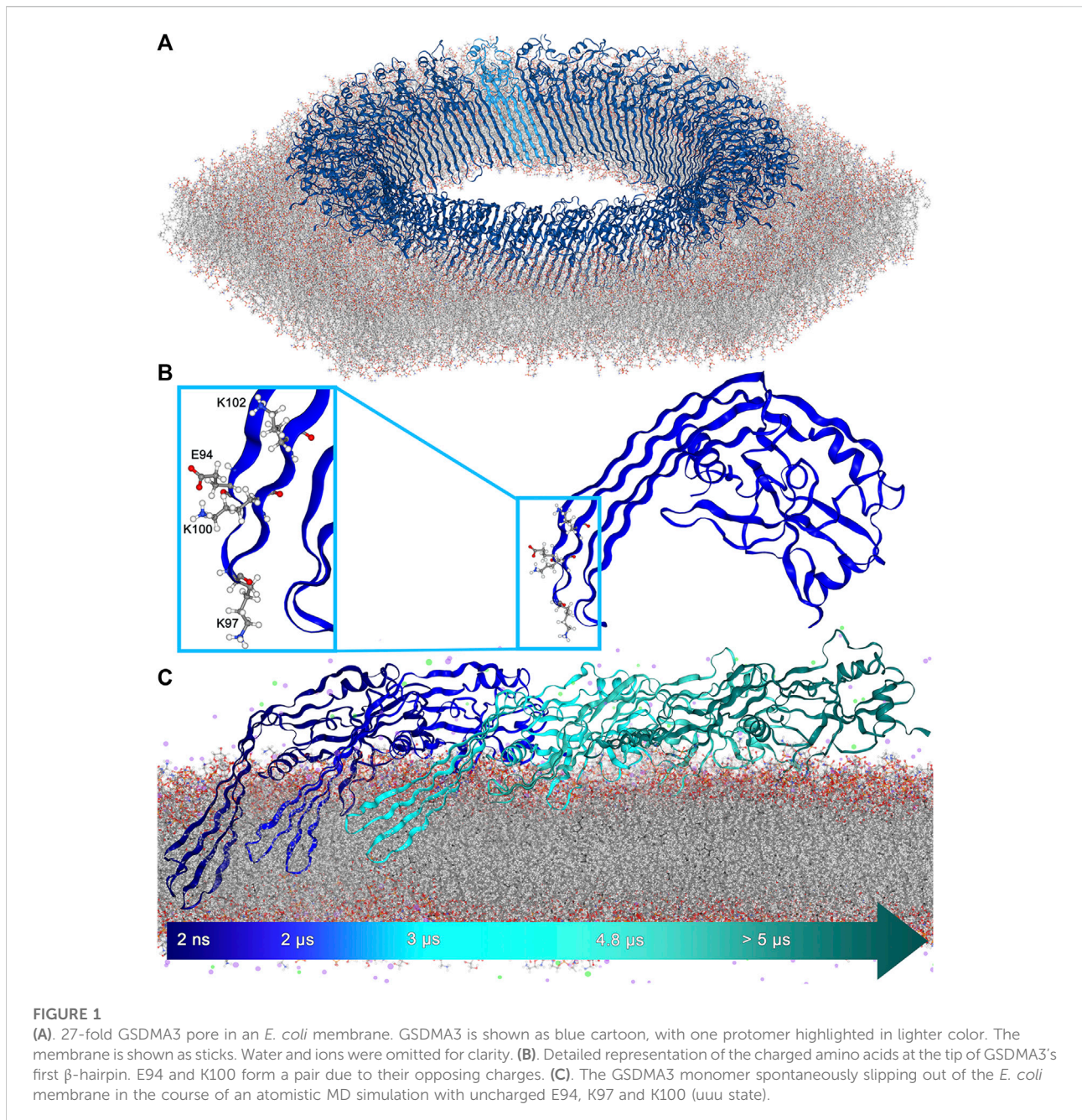
Gasdermins execute programmatory cell death, known as pyroptosis, by forming medium-sized membrane pores. Recently, the molecular structure of those pores as well as the diversity in their shape and size have been revealed by cryoTEM and atomic force microscopy, respectively. Even though a growth of smaller to larger oligomers and reshaping from slits to rings could be documented, the initiation of the gasdermin pore formation remains a mystery. In one hypothesis, gasdermin monomers insert into membranes before associating into oligomeric pores. In the other hypothesis, gasdermin oligomers preassemble on the membrane surface prior to membrane insertion. Here, by studying the behavior of monomeric membrane-inserted gasdermin-A3 (GSDMA3), we unveil that a monomeric gasdermin prefers the membrane-adsorbed over the membrane-inserted state. Our results thus support the hypothesis of oligomers preassembling on the membrane surface before membrane penetration. At the same time, our simulations of small membrane-inserted arcs of GSDMA3 suggest that the inserting oligomer can be small and does not have to comprise a full ring of approximately 26–30 subunits. Moreover, our simulations have revealed an astonishingly large impact of salt-bridge formation and protein surroundings on the transmembrane passage of charged residues, reducing the energetic cost by up to 53% as compared to their free forms. The here observed free energy barrier of mere 5.6 kcal/mol for the membrane insertion of monomeric GSDMA3 explains the surprising ability of gasdermins to spontaneously self-insert into cellular membranes.

KEYWORDS

gasdermin, membrane proteins, free energy, molecular dynamics, computational biology, membrane pore, protein insertion

1 Introduction

Gasdermins (GSDMs) are a protein family conserved among vertebrates, including mice, rats, horses, and humans, where they play a central role in defense mechanisms eliminating harmful cells through pyroptosis [Shi et al. \(2017\)](#). Pyroptosis is a proinflammatory form of programmed cell death [Walle and Lamkanfi \(2016\)](#)



following a range of pathways, either the canonical or non-canonical inflammasome pathway, where the inflammasomes detect cytosolic contamination [Kovacs and Miao \(2017\)](#), or via granzymes. In the final step of pyroptosis, transmembrane lytic pores are formed causing swelling of the cell, followed by the efflux of cytoplasmic content, and cell rupture [Zahid et al. \(2021\)](#). Recently, GSDMs have been shown to be the sole executors of pyroptosis by forming lytic pores [Kovacs and Miao \(2017\)](#).

Before revealing its full necrotic potential, gasdermin lies dormant in a deactivated form consisting of covalently bound C- and N-terminus. Across all variants, the three-dimensional structure is very similar, despite diverging sequences (45% homology [Zahid et al. \(2021\)](#)). Upon inflammation, enzymatic cleavage of gasdermins releases the functional N-terminus of its inhibitory C-terminus, enabling membrane insertion and pore formation. [Ding et al. \(2016\)](#) While human GSDMD can be cleaved by inflammatory caspases 1, 4, 5, and 11 [Shi et al. \(2015\)](#),

the specific protease responsible for the cleavage of GSDMA3 remains a mystery.

Gasdermins are involved in a wide range of diseases [Liu et al. \(2021\)](#). GSDMA is associated with and presumably involved in asthma, systemic sclerosis, alopecia, and inflammatory bowel disease [Lluis et al. \(2011\)](#); [Yu et al. \(2011\)](#); [Saeki et al. \(2009\)](#); [Terao et al. \(2017\)](#); [Söderman et al. \(2015\)](#). Also, pyroptosis is surmised to be stimulated in SARS-CoV-2 infections through the non-canonical inflammasome [Lee et al. \(2020\)](#); [Zheng et al. \(2020\)](#). In mice, GSDMA3 is expressed in skin cells and hair follicles [Runkel et al. \(2004\)](#) and is involved in apoptosis [Lei et al. \(2011\)](#) and differentiation [Li et al. \(2010\)](#). Moreover, due to the ability of gasdermins to self-insert into specific membranes independent from insertases and chaperones [Ding et al. \(2016\)](#), GSDMA3 is being researched as a therapeutics specifically disrupting cancer cells and thereby reduce tumor growth [Wang et al. \(2020\)](#).

The molecular structure of the gasdermin lytic pore was resolved first in 2018, when [Ruan et al. \(2018\)](#) published the cryoTEM structure of gasdermin-A3 pores, presenting highly structured β -barrel oligomers consisting of 26–28 monomers, among which the 27-fold pore ([Figure 1A](#)) was the most common. Three years later, human gasdermin-D has been shown to preferably form β -barrels comprising 33 protomers [Xia et al. \(2021\)](#). Recently, extensive atomic force microscopy (AFM) investigations have shed light on the growth of gasdermin pores [Mulvihill et al. \(2018\)](#); [Mari et al. \(2022\)](#) and by combining AFM with molecular dynamics (MD) simulations, the opening of the lytic pore by release of the lipids (and proteins) from the center of the oligomer was visualized [Mari et al. \(2022\)](#). Nevertheless, the compelling issue whether gasdermins insert into the membrane and then assemble pores, or whether the membrane-adsorbed oligomers obtained both by AFM and cryoTEM are able to tear into the membrane, remains open.

Usually, membrane proteins insert into the hydrophobic membrane core guided and aided by their hydrophobic domains [Ulmschneider et al. \(2014\)](#); [Brambillasca et al. \(2005\)](#). Yet, an increasing number of membrane proteins have been discovered, which contain multiple polar or even charged amino acid residues in their membrane inserting domains [Broecker et al. \(2014\)](#); [Vögele et al. \(2019\)](#); [Altrichter et al. \(2017\)](#); [Brambillasca et al. \(2006\)](#); [van Dalen and de Kruijff \(2004\)](#); [Mulvihill et al. \(2015\)](#), many of them containing or forming β -barrel pores with hydrophilic residues inside the pore and hydrophobic ones on the outside of the pore where they are in contact with the membrane [Bosshart et al. \(2012\)](#); [Vögele et al. \(2019\)](#); [Altrichter et al. \(2017\)](#); [Mulvihill et al. \(2015\)](#). A non-negligible number of membrane proteins is able to self-insert. [Broecker et al. \(2014\)](#); [Vögele et al. \(2019\)](#); [Bosshart et al. \(2012\)](#) However, as the membrane passage of charged amino acids comes at a very high energetic cost [MacCallum et al. \(2007\)](#); [Johansson and Lindahl \(2009\)](#), insertases like YidC and

SecYEG typically aid the process [Laskowski et al. \(2021\)](#); [Oswald et al. \(2021\)](#). The more astounding it is that GSDMA3 self-inserts, as four charged residues, one glutamic acid (E94), and three lysines (K97, K100, and K102) ([Figure 1B](#), [Supplementary Figure S2](#)) have to pass, or in case of K102 at least partially insert into the hydrophobic membrane core, during the protein's insertion process. Other members of the gasdermin family, including the functionally very significant human GSDMD, possess β -hairpins decorated with even more polar and charged residues ([Supplementary Figures S3–S5](#)). A couple of mechanisms have been suggested before to aid the insertion of charged amino acids into hydrophobic membrane cores: The formation of water defects where water molecules surround polar and charged residues inside the membrane [Ulmschneider \(2017\)](#); [Wang et al. \(2014\)](#); [Allolio et al. \(2016\)](#); [Dorairaj and Allen \(2007\)](#); [Bonhenry et al. \(2013\)](#); [Li et al. \(2013\)](#), the bending of lipids enabling polar and charged headgroups (e.g. phosphates) to stabilize residues of opposing charge [Allolio et al. \(2016\)](#); [Dorairaj and Allen \(2007\)](#); [Li et al. \(2013\)](#), salt-bridge formation between residues of opposing charges [Duart et al. \(2022\)](#); [Mbaye et al. \(2019\)](#); [Chin and von Heijne \(2000\)](#); [Donald et al. \(2011\)](#), “piggyback” where one charged residue drags water into the membrane and thereby paves the way for membrane insertion of further charged residues at hardly any extra cost [MacCallum et al. \(2007, 2008\)](#), with arginine and its guanidinium cation presenting a special case titled “arginine magic” [Vazdar et al. \(2018\)](#); [Allolio et al. \(2016\)](#); [Moon and Fleming \(2011\)](#), as well as mediating effects of the protein surroundings that provide charge shielding and stabilization [Bosshart et al. \(2012\)](#); [Vögele et al. \(2019\)](#); [Altrichter et al. \(2017\)](#); [Moon and Fleming \(2011\)](#); [Cymer et al. \(2015\)](#); [van Dalen and de Kruijff \(2004\)](#).

To determine the energetic cost of GSDMA3 membrane insertion, we conducted extensive molecular dynamics simulations of its N-terminus with four charge combinations regarding the membrane-passing residues E94, K97 and K100. Our simulations have revealed that the salt-bridge formation between E94 and K100 and the polar protein surroundings of all three charged residues drastically decrease the energy barrier for membrane insertion of GSDMA3's β -hairpins, in comparison to the insertion cost of individual charged amino acids.

2 Methods

The membrane-inserted structure of the N-terminus of murine gasdermin-A3 was based on the recently published cryoTEM structure (rcsb code 6CB8 [Ruan et al. \(2018\)](#)). Modeller 9 [Webb and Sali \(2016\)](#) was used to insert the missing residues 66-PGSS-69 and 234-KIRR-237 to obtain a full pore-forming version of the protein characterized in detail previously [Mari et al. \(2022\)](#). Additionally, two membrane-adsorbed models were prepared. In the first model, termed “pre-inserted”, the β -hairpins (residues F81-L113 and V164-

I198) were remodelled as loops by Modeller 9. In the “cleaved” model, the N-terminal half (residues M1-R237) of the X-ray structure 5B5R Ding et al. (2016) of full-length GSDMA3 was extracted and missing residues added by Modeller 9. The monomeric proteins were then inserted into or adsorbed onto an *E. coli* polar lipid extract bilayer Pluhackova and Horner (2021), consisting of 14 different lipids containing 72% phosphatidylethanolamine (PE), 23% phosphatidylglycerol (PG) and 5% cardiolipin lipids with 37% of saturated, 25% cyclopropanylated, and 38% unsaturated lipid tails, using our established multiscaling procedure Pluhackova et al. (2013). First, the simulation system was prepared and equilibrated at coarse-grained resolution, using the Martini3 force field Souza et al. (2021). Then the system was converted to all-atom resolution using backward Wassenaar et al. (2014) and the CHARMM36 forcefield Huang et al. (2017); Klauda et al. (2010) with the TIP4P water model Jorgensen and Madura (1985) as described in the original implementation of the CHARMM force field in GROMACS Bjelkmar et al. (2010) and reequilibrated atomistically. All simulations were performed in GROMACS (2018.x - 2021.x) Abraham et al. (2015). For more details see Supplementary Information, section Supplementary methods.

3 Results

The structure of the transmembrane lytic pore formed by GSDMA3 Ruan et al. (2018) (Figure 1A) shows a typical distribution of hydrophobic side chains on the membrane-facing side of the β -barrel and hydrophilic (polar and charged) residues on the water facing surface of the β -barrel Wimley (2002). Following the hypothesis that individual GSDMA3 proteins insert into the membrane and then oligomerize Mulvihill et al. (2018), both the hydrophobic and hydrophilic sides of the monomeric GSDMA3's β -hairpin face the membrane lipids. Especially the membrane insertion and incorporation of the first β -hairpin is supposed to be energetically unfavorable, as it is decorated by multiple charged residues (Supplementary Figure S2): one lysine in position 102 and two further lysines and one glutamic acid at the tip (E94, K97 and K100) (Figure 1B).

In order to shed light on the behavior and positioning of the monomeric GSDMA3 adsorbed onto or embedded in a well characterized membrane, where GSDMA3 is known to spontaneously insert into and form oligomers in Mari et al. (2022), we have inserted the GSDMA3 monomer into a model of an *E. coli* polar lipid extract membrane Pluhackova and Horner (2021). This membrane choice is further justified by the facts that GSDMA3 is lethal to bacteria, including *E. coli* Ding et al. (2016) and ruptures mitochondrial membranes of similar lipid composition Rogers et al. (2019). Moreover, in order to unravel the impact of charged residues on the estimated

properties, we have varied the protonation state of the three titratable residues at the tip of the first hairpin in our atomistic molecular dynamics simulations (E94, K97, and K100 charged (ccc), all three uncharged (uuu), and E94 and K100 charged but K97 uncharged (cuc)). In the geometric perturbation simulations, the ucu state (E94 and K100 uncharged but K97 charged) was added for comparison purposes. In the membrane-adsorbed state, the orientation of GSDMA3 on the membrane surface stays conserved during the course of the simulations, while the protein diffuses around. The disordered loops, forming β -hairpins in the pore state, sample the conformational space, and temporarily attach to the membrane surface. However, even though a few residues penetrated the membrane/solvent interface, no spontaneous insertion was observed, similarly to recent MD simulations of GSDMD Schaefer and Hummer (2022). Therefore, in the following we concentrate on the behavior of membrane-inserted GSDMA3. During the equilibration phase, the position of the protein in the membrane was restrained to the lytic-pore conformation. This caused water entering the bilayer along the β -hairpins and lipid deformation in the vicinity of the hydrophilic face of the protein (Figures 2A,E). Upon releasing the restraints in the production run simulations the β -hairpins started to reshape and reposition, independently of the protein's protonation state, in an attempt to minimize the membrane defects (Figures 2B–D). The second β -hairpin, carrying no charged residues, assumed a twisted conformation and left the headgroup region of the extracellular leaflet shifting to the hydrophobic membrane core. This ductile form enabled the monomeric protein to remain membrane-inserted (Supplementary Figures S6–S8) for the simulation time (ranging from 5 to 12.8 μ s), except for one uuu simulation, in which the β -hairpins slipped out of the bilayer after 5 μ s (Figure 1C, Supplementary Figure S8). Supplementary Figure S9 shows the increased flexibility of the β -hairpins compared to the globular domain by coloring the monomeric GSDMA3 according to the B-factors of the C_{α} atoms. In those simulations, as well as in additional simulations of GSDMA3 adsorbed on the membrane surface in a prepore or cleaved state (i.e. with β -hairpins modelled as loops) lasting 5 and 1 μ s, respectively, the orientation of the GSDMA3 on the membrane surface and the protein-lipid interactions attaching the globular domain of GSDMA3 to the membrane remained the same as observed in the lytic-pore state Mari et al. (2022); Ruan et al. (2018).

In the membrane-inserted state of monomeric GSDMA3, the first β -hairpin stays deeply inserted and K97, regardless of its charge, anchors the hairpin to the lipid headgroups of the extracellular leaflet causing a membrane dent (Figure 2G). K102 bends to the lipid headgroups of the intracellular membrane leaflet (Figure 2H). Such lysine bending from the hydrophobic membrane core to the polar lipid headgroups has been observed before Pluhackova et al.

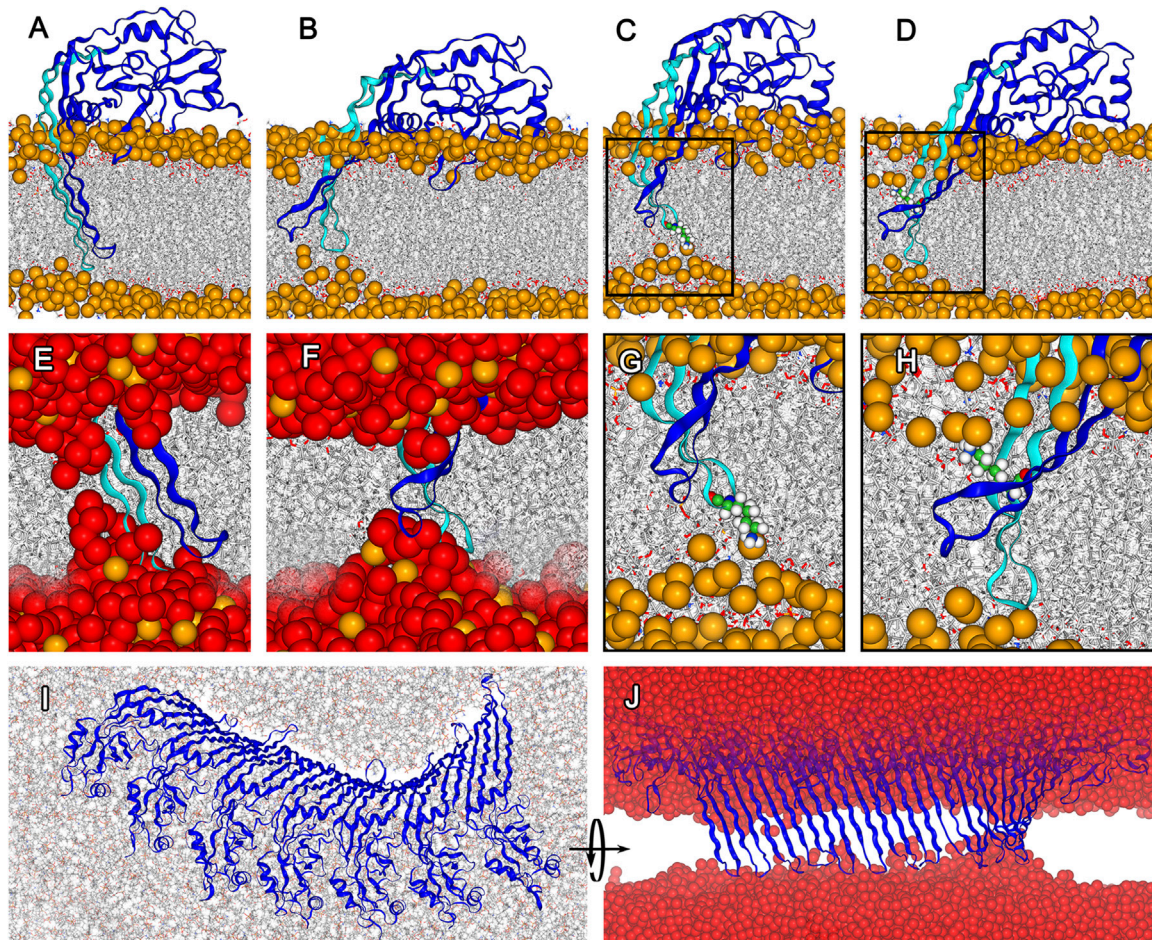


FIGURE 2

Structural adaptation of membrane inserted GSDMA3 in a monomeric state and forming an arc comprising 7 protomers. (A). Conformation of monomeric GSDMA3 in the beginning of the production run simulations (i.e. at 0 μ s). (B). Reshaping of the β -hairpins of monomeric GSDMA3 after 5 μ s of simulation time. (C). K97 (highlighted as small spheres) anchors the GSDMA3 monomer to the lipid headgroups in the extracellular membrane leaflet. (D). Snorkeling of K102 (shown as small spheres) into the lipid headgroups of the cytosolic membrane leaflet. (E). Zoom-in on the water defect at 0 μ s and (F) after 5 μ s. (G). Detail view on K97 anchoring from (C). (H). Detail view on K102 snorkeling in (D). (I). Cytosolic view on the deformation of 7-mer arc after 4 μ s and (J) a detail on the β -hairpins of the 7-mer arc pulling water into the membrane. GSDMA3 is shown as blue cartoon, in (A)–(H) the first β -hairpin carrying the charged residues is highlighted in cyan. The membrane is shown as grey sticks with phosphorus atoms highlighted as orange spheres (only in (A)–(H)). Water is shown in (E), (F), and (J) as red spheres. Apart from (I), the cytosolic side is found on the top and the extracellular side on the bottom of the membrane. In all here presented simulations, GSDMA3 was in its ccc state (i.e. K97, K100, and E94 were charged).

(2015); Mishra et al. (1994) and is called “lysine snorkeling” Strandberg and Killian (2003). In the simulations with charged E94 and K100 (i.e. fully charged ccc and partially charged cuc states, with K97 being neutral in the latter case) K97 is deeply inserted (average distance between the C_{α} of K97 and the membrane center of mass after exclusion of the first 500 ns simulation time for equilibration purposes amounts to -0.60 ± 0.27 nm for ccc and -0.68 ± 0.27 nm for cuc. The error given represents the standard deviation of the distribution and thus the fluctuations of the insertion depth (Supplementary Figures S6, S7). In case of the uuu

simulations, both hairpins translate towards the hydrophobic membrane core (-0.27 ± 0.44 nm, Supplementary Figure S8). This positioning of both β -hairpins in the membrane core enabled the β -hairpins to slip out of the membrane in one replica of the uuu simulations, leaving the GSDMA3 monomer adsorbed on the membrane surface. Such behavior of the GSDMA3 monomer made us wonder how the process of membrane excision looks like from an energetic perspective and how the charges of the three amino acids at the tip of one β -hairpin influence the free energy landscape and therefore the membrane passage process.

Using structures from the previous simulations in which the β -hairpins of GSDMA3 are 1) in the transmembrane state, 2) slipping out of the bilayer, and 3) adsorbed on the bilayer surface (Supplementary Table S1) we have performed “umbrella” (geometric perturbation) sampling simulations and constructed the potential of mean force (PMF) describing the excision/insertion of GSDMA3 β -hairpins from/into the membrane, along the reaction coordinate ζ represented by the z-distance between the C_α of K97 and the center of mass of the bilayer. Thus, we could avoid including structures and conformations from far-from-equilibrium steered molecular dynamics simulations, which pose often a problem in terms of convergence and accuracy of PMF estimation Blazhynska et al. (2022). However, one has to keep in mind that even though the above mentioned structures overlap over the whole span of our reaction coordinate, we can not assure to be sampling the complete conformational space exhaustively. Nevertheless, the convergence of our PMFs and the comparably small error bars support the following statements. The PMFs revealed two local minima (Figures 4LJ, Supplementary Figure S10). The minimum at $\zeta \approx 2$ nm corresponds to the membrane-adsorbed state of the β -hairpins. In this state, many polar and charged residues (mainly K97) form energetically favorable interactions with intracellular lipid headgroups (Supplementary Figures S23–S25). The second minimum, at $\zeta \approx -0.25$ nm, corresponds to the transmembrane state of the β -hairpins of GSDMA3. In this state, K97 is interacting with the lipid headgroups in the extracellular membrane leaflet (Supplementary Figure S23). A maximal energy barrier between these two minima, corresponding to the cost of the insertion/excision, amounted to 5.57 kcal/mol in the ccc simulation. While this barrier agrees perfectly with the experimental value of the free energy required for membrane insertion of lysine in context of a transmembrane β -barell OmpLA amounting to 5.39 ± 0.52 kcal/mol Moon and Fleming (2011), it contrasts with the energy barrier that a single charged lysine (10.15 kcal/mol), or charged lysine analog (7.46 kcal/mol) experiences when passing the bilayer (Figure 4K, Supplementary Figures S15, S16, S21, S22). These values are smaller than those obtained previously by MacCallum et al., who have predicted a barrier of almost 15 kcal/mol for a charged lysine side chain analog (described by the OPLS-AA force field Kaminski et al. (2001); Rizzo and Jorgensen (1999)) passing the DOPC bilayer (described by the Berger force field Berger et al. (1997)) MacCallum et al. (2007). Similarly, Sandoval-Perez and Pluhackova et al. have observed an energy barrier of 14 kcal/mol for a charged lysine residue including a backbone capped with acetyl on the N-terminus and an amine group on the C-terminus passing a POPC bilayer (all described by the CHARMM36 force field) Sandoval-Perez et al. (2017). Our values of 10.15 and 7.46 kcal/mol thus suggest that 1) the negatively charged *E. coli* PLE bilayer makes an insertion of a positively charged lysine molecule a little more favorable than the

zwitterionic POPC bilayer, 2) self-insertion of positively charged sole lysine into this membrane is highly improbable under physiological conditions, and 3) the protein surroundings of the lysine drastically reduce its free energy insertion barrier.

Visual investigation of the trajectories gave first hints on differences in membrane deformations and water defects regarding the β -hairpin versus the lysine-only passage through the bilayer. Due to the too high dewetting cost, the charged lysine pulls 18.5 and the analog 7.9 water molecules into the bilayer (averaged over $-1 \leq \zeta \leq 1$) and exposes them to the hydrophobic membrane core (Supplementary Figures S26, S27), which is known to be energetically costly Wang et al. (2014). In Figure 3, the even larger defects formed by GSDMA3 regardless of its charge state are shown. When the protein is fully inserted, it pulls in water molecules from both intra- and extracellular surroundings. Thereby the polar surface of the β -hairpins accommodates on average 18.5, 17.0, 13.0, and 14.0 water molecules in the ccc, cuc, ucu, and uuu states, respectively, in the hydrophobic center of the membrane ($-1 \leq \zeta \leq 1$). Very rarely a single ion briefly diffused into the water defects inside the hydrophobic membrane core.

However, in the case of GSDMA3 not only one lysine but four charged residues and a number of polar residues (Supplementary Figure S2) have to insert into the bilayer for the β -hairpin to reach the membrane-inserted state. Two of those residues, E94 and K100, often formed a salt-bridge in our simulations (Figure 4L), therefore they were charge-neutralized pairwise. The PMF curves show that the charge of the E94-K100 pair has only a marginal impact on the height of the energy barrier and on the position and depth of the two energy minima. Figure 4L shows that the deeper these two residues are inserted in the membrane, the closer they stay together. In their charged state, E94 and K100 form a salt bridge (indicated by a distance shorter than 0.4 nm), but even in their neutral form, polar interactions keep E94 and K100 close together. Such close contact isolates the (partial) charges from the surroundings, effectively shielding them from the hydrophobic membrane core. Moreover, it can be supposed that the interaction between E94 and K100 contributes to the stability of the β -hairpin. Comparing the PMFs with varying charge on K97 (Figures 4L, J) reveals that the charge of this residue mainly determines the relative depth of the two minima and thus the preference of GSDMA3's β -hairpin for the membrane-adsorbed or the membrane-inserted state: If K97 is charged (ccc, ucu), the membrane-adsorbed state is preferred over the transmembrane state and vice-versa. Shifting the PMF curve in the cuc (relative to ccc) and uuu (relative to ucu) states at maximum ζ (where K97 is found in the solvent) by the free energy required to deprotonate a lysine residue in bulk water at pH 7.0 MacCallum et al. (2008); Johansson and Lindahl (2009), allows us to estimate whether the K97 uncharged state is more favorable at some insertion

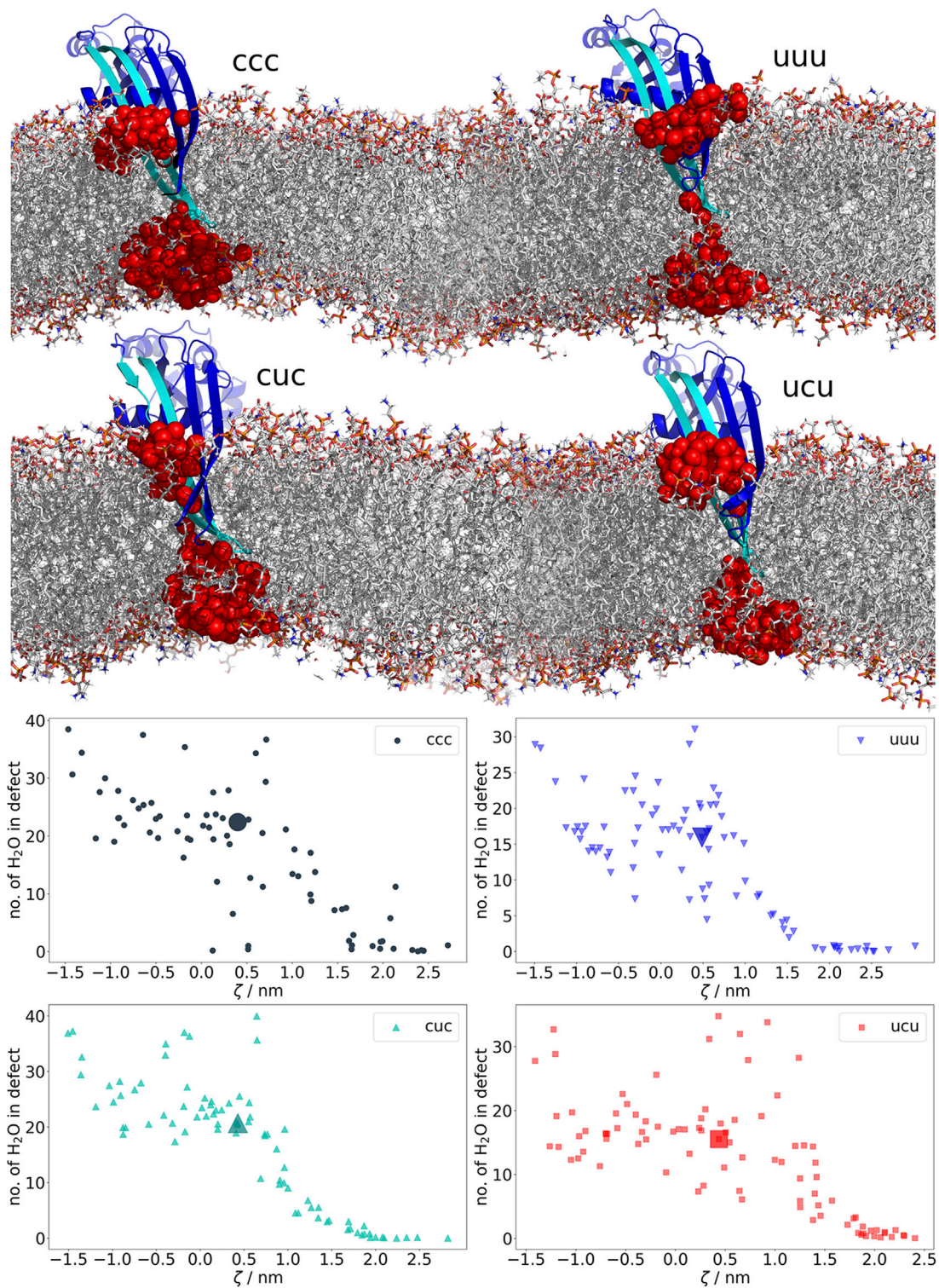
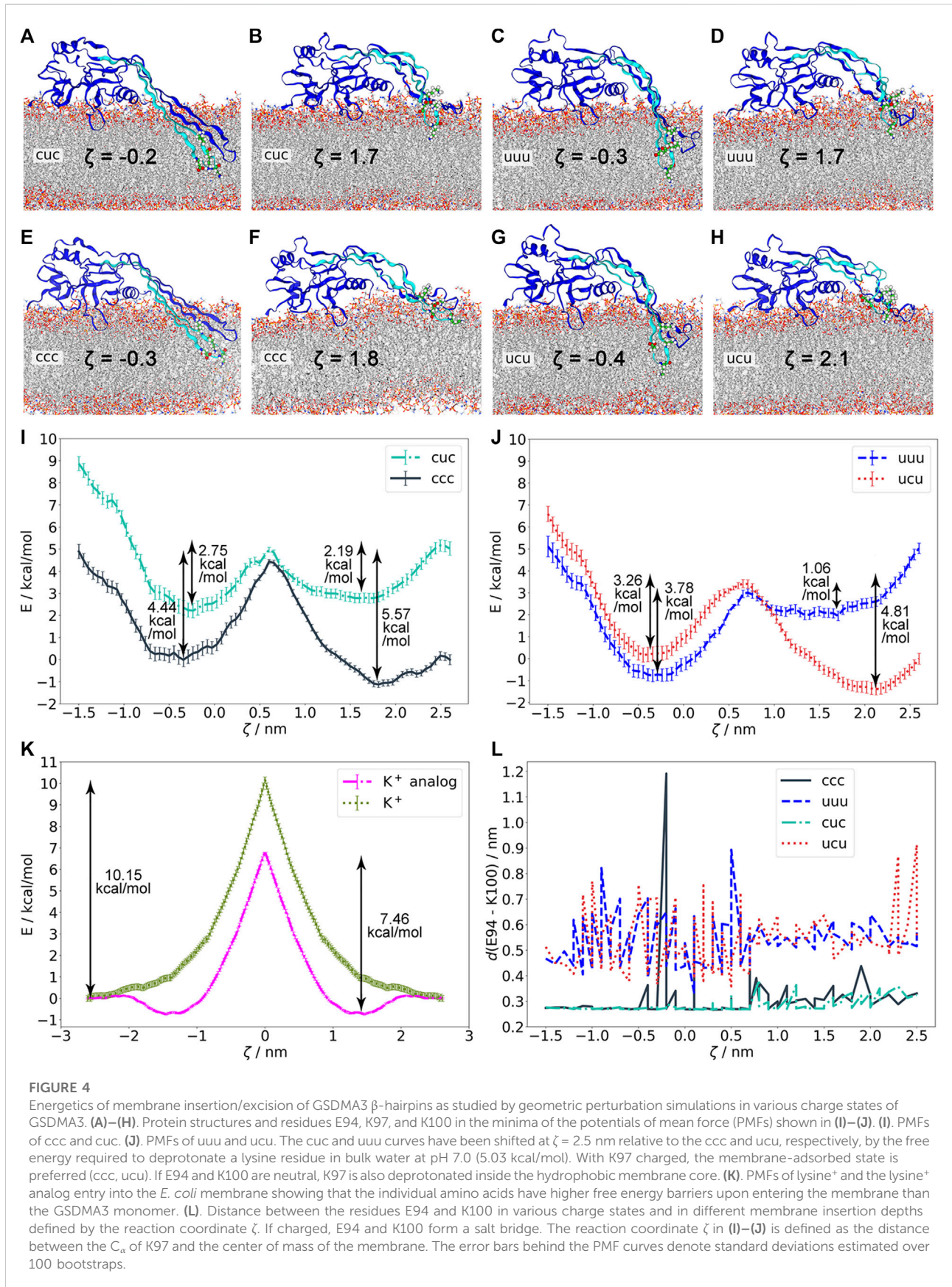


FIGURE 3

Water-filled membrane defects caused by β -hairpins of GSDMA3. The plots at the bottom show the average number of water molecules in the defect in each trajectory from the geometric perturbation. Coloring of the datapoints is based on the charges of E94, K97, and K100 (u = uncharged, c = charged). As soon as GSDMA3 comes into contact with the membrane at $\zeta \approx 2$, water-filled membrane defects arise. The highlighted large datapoints correspond to the visualized structures above. In the molecular representations, water oxygens in membrane defects are shown as red spheres. GSDMA3 is visualized as blue cartoon, with the first β -hairpin highlighted in cyan. The membrane is shown as sticks.



depth than the charged state, which is prevalent in aqueous solution (Figure 4). As the curves of cuc and ccc never cross and the latter state is lower in energy in solution, the ccc state is preferred over the cuc state even in the membrane hydrophobic core, despite its higher insertion barrier (5.57 kcal/mol vs. 2.19 kcal/mol). Considering the shapes of the PMFs for uuu and ucu (Figure 4J), it is evident that the uuu curve shows hardly any barrier (1.06 kcal/mol) within the membrane core and has a deeper minimum (3.78 kcal/mol) than the ucu curve (3.26 kcal/mol) in the membrane inserted state. Interestingly, after shifting the uuu curve relative to the ucu PMF curve in solution by the deprotonation free energy of K97 (5.03 kcal/mol), it appears that contrary to the cuc state, K97 prefers to be neutralized if inserted deep in the hydrophobic membrane core. Obviously, synergistic effects between the E94-K100 pair and K97 exist. Yet, the uuu and ucu states are energetically much less favorable than the ccc and cuc states (Supplementary Figure S10) and thus do not represent physiologically relevant states of membrane inserted GSDMA3.

Salt bridge formation leads to even more extreme pKa values of the involved amino acids, i.e. the pKa of acids is reduced and that of bases increased Yang et al. (1993). The more the pKa deviates from the pH of interest (here 7), the larger is the neutralization free energy which is defined as $\Delta G \approx \pm (2.303RT) \cdot (\text{pKa} - \text{pH})$. Therefore, the sum of neutralization free energies of individual K97 ($\Delta G = 4.35$ kcal/mol Johansson and Lindahl (2009)), E94 ($\Delta G = 4.02$ kcal/mol Johansson and Lindahl (2009)), and K100 ($\Delta G = 4.35$ kcal/mol Johansson and Lindahl (2009)), i.e. 12.39 kcal/mol, represents the lowest boundary of the free energy difference between the ccc and uuu PMF curves in solution. Thus, neither the ucu nor the uuu PMF curve will ever cross the ccc PMF curve, which obviously represents the most stable state. Therefore, our simulations show that even though individual amino acids are expected to neutralize in the hydrophobic core of the membrane MacCallum et al. (2007); Sandoval-Perez et al. (2017), amino acids which are part of a complex protein do not necessarily have to do so. Concludingly, our findings suggest that neither K97, nor K100 and E94 neutralize upon membrane insertion of GSDMA3 β -hairpins and monomeric GSDMA3 favors the membrane-adsorbed over the membrane-inserted state. In order to support this hypothesis, we have investigated in detail our recent simulations of arcs consisting of seven GSDMA3 protomers in the *E. coli* PLE membrane Mari et al. (2022). The simulations lasting 2.5 and 4 μs show that even though the overall shape of the arc changes slightly, with the C-terminal part of the oligomer twisting pronouncedly (Figure 2I), the transmembrane orientation of the GSDMA3 protomers mostly resembles the conformation in the cryoTEM pore. However, the protomers at the edges, especially at the C-terminal end where the second hairpin is not stabilized by H-bonds to the neighboring chain, leave the rigid pore conformation. This adaptation is clearly indicated by small root mean square deviations (RMSD) of the hairpins relative to the cryoTEM structure in the center of the arc and increasing

RMSDs at the ends of the arc (Supplementary Figure S28). Moreover, the C-terminal end exhibits larger RMSDs. More detailed analysis revealed that both the β -sheets and the hairpin tips contribute, albeit the tips' RMSD is always larger in agreement with their higher structural plasticity. In the beginning of the simulations, when the GSDMA3 protomers were position restrained to the conformation in the cryoTEM pore, water defects were present along the whole arc. After 4 μs the tips and the side chains at the polar side of the hairpins reoriented so that the only water defect is present at the twisted C-terminal end of the arc (Supplementary Figures S29–S32).

All our findings taken together suggest that GSDMA3 pre-assembles pores on top of a lipid membrane prior membrane insertion, during which all titratable residues on the GSDMA3's β -hairpins retain their charged state.

4 Discussion

Recently, cryoTEM Ruan et al. (2018), AFM experiments Mari et al. (2022) and multiscale MD simulations Mari et al. (2022) have shed light on the shape and growth of GSDMA3 oligomers and their pre-pore to pore transition by (lipid) unplugging. Nevertheless, because the membrane insertion of gasdermins succeeds without a vertical collapse of the protein, which is characteristic e.g. for pneumolysin van Pee et al. (2016), perforingolysin O Czajkowsky et al. (2004), or suliyisin Leung et al. (2014), the initial step of GSDMA3 pore formation consisting of oligomerisation and membrane insertion and their timely order remained hidden. Here, our extensive all-atom MD simulations of the GSDMA3 monomer and the energetics of its membrane insertion have revealed that the pore-forming N-terminus of GSDMA3 prefers the membrane-adsorbed over the membrane-inserted state if the protein is in its monomeric form. Such membrane-adsorbed GSDMA3 monomers explain the small dots observed in time-lapse AFM in our recent study Mari et al. (2022), which are present only in case of both the protease TEV and GSDMA3 in solution without rinsing. As these dots do not appear in controls containing either full-length GSDMA3 lacking the protease or the protease only, they must be comprised by cleaved GSDMA3. Also their disappearance after rinsing by a buffer solution, which also removes membrane adsorbed pre-pore rings from the membrane surface, indicates that the dots capture adsorbed instead of inserted GSDMA3 monomers or small oligomers. These findings support the hypothesis that GSDMA3 oligomers preassemble on the membrane surface prior to membrane insertion and pore formation. The required minimal size and preferred shape of those oligomers for their spontaneous membrane insertion as well as molecular details on the insertion pathway remain to be unraveled.

At the same time, our simulations have unveiled interesting aspects of the membrane passage of charged amino acids in the protein context. Membrane insertion of protein-attached charged amino acids appears to have completely different energetics than the membrane passage

of individual amino acids or their side chain analogs. This is true for both single charged amino acids as well as their pairs. Astonishingly, the charge of the amino acid pair E94 and K100 does neither affect the preferred minimum of the protein on or in the membrane, nor does it significantly impact the energy barrier for membrane insertion/excision of GSDMA3's β -hairpins. These observations hint to the fact that salt bridge formation of nearby amino acids together with their protective protein surroundings shield the charged residues from the hydrophobic membrane core, thus helping GSDMA3 to insert and settle in the membrane. A recent publication has shown that a salt bridge between a charged lysine and glutamic acid is most stable under intermediate microhydration, as it can be found in water-solvated protein cavities [Pluhařová et al. \(2012\)](#), or in our case, in water-filled membrane defects. Also, the energy barrier for the membrane passage of K97, localized at the tip of the first β -hairpin, appears to be significantly reduced (5.57 and 4.81 kcal/mol if K97 is positively charged) compared to the membrane insertion of a charged lysine (10.15 kcal/mol) or a charged lysine analog (7.46 kcal/mol) alone. Thereby, the energy barrier of the membrane insertion of GSDMA3's β -hairpins in their completely charged state (5.57 kcal/mol) agrees astonishingly well with the energy cost of membrane insertion of a lysine residue located centrally on a transmembrane β -barrel of OmpLA (5.39 kcal/mol) [Moon and Fleming \(2011\)](#). Even smaller energy barriers for membrane passage were observed for simulations with deprotonated K97 (i.e. cuc and uuu states). Our extensive equilibrium simulations allowed us to even observe a spontaneous passage of the β -hairpins in the uuu state over the bilayer. Even though the protein thus switched to an energetically less favorable membrane-adsorbed state (in case of the uuu charge state) the observation of this rare event goes hand in hand with the comparably low energy barrier for membrane insertion of GSDMA3. We thus hypothesize that the insertion capability of GSDMA3 is likely to be modulated by molecules stabilizing the membrane-inserted or the membrane-adsorbed state of the protein, e.g. membrane composition or transmembrane proteins. As mentioned elsewhere, the discrepancies between the calculated and experimental insertion free energies of individual charged amino acids or charged amino acids in a protein context result from different microscopic environments rather than from methodological errors [Gumbart and Roux \(2012\)](#). The high energy barrier for the membrane transition of charged amino acids is typically accounted to the formation of water-filled defects reaching into the hydrophobic membrane core [Ulmschneider \(2017\)](#); [Wang et al. \(2014\)](#); [Allolio et al. \(2016\)](#); [Dorairaj and Allen \(2007\)](#); [Bonhenry et al. \(2013\)](#); [Li et al. \(2013\)](#). Here, we observe similar water defects upon the membrane insertion of GSDMA3's β -hairpins. Obviously, the polar and charged

amino acids on the hydrophilic face of the hairpins stabilize the water inside the membrane, thus lowering the energy barrier for the membrane passage of charged amino acids similarly to the mechanism used by the passive membrane insertase YidC [Chen et al. \(2022\)](#). In summary, protein surroundings significantly aid the membrane insertion of charged amino acids by 1) providing a microhydrating environment around charged residues through stabilizing water-filled membrane defects, 2) enabling pair formation between oppositely charged residues, and 3) shielding charged residues from the hydrophobic membrane core. As polar and charged residues cooperate upon membrane insertion in a "piggyback" [MacCallum et al. \(2007\)](#) manner rather than contributing individually to the energy barrier, such nonadditivity poses a challenge for the applicability of hydrophobicity scales predicting membrane-insertion energies of transmembrane proteins.

Data availability statement

The raw data supporting the conclusions of this article will be made available by the authors, without undue reservation.

Author contributions

KP has conceptualized the research, both authors have performed and analyzed the simulations, both authors have interpreted the results and written the article.

Funding

VK and KP are funded by Deutsche Forschungsgemeinschaft (DFG, German Research Foundation) under Germany's Excellence Strategy-EXC 2075-390740016.

Acknowledgments

The authors are grateful to Daniel J. Müller, Stefania A. Mari and Andreas Engel for wonderful discussions on the life of gasdermins and Sandro Keller for an insightful debate on the impact of charged residues on spontaneous membrane insertion. We acknowledge the support by the Stuttgart Center for Simulation Science (SimTech). The molecular dynamics simulations were performed on the supercomputers Piz Daint at the Swiss National Supercomputing Centre (CSCS) under project ID s945 and on BwForCluster BiNAC funded by the Ministry of Science, Research and the Arts Baden-Württemberg and by the Federal Ministry of Education and Research.

Conflict of interest

The authors declare that the research was conducted in the absence of any commercial or financial relationships that could be construed as a potential conflict of interest.

Publisher's note

All claims expressed in this article are solely those of the authors and do not necessarily represent those of their affiliated

organizations, or those of the publisher, the editors and the reviewers. Any product that may be evaluated in this article, or claim that may be made by its manufacturer, is not guaranteed or endorsed by the publisher.

Supplementary material

The Supplementary Material for this article can be found online at: <https://www.frontiersin.org/articles/10.3389/fcell.2022.958957/full#supplementary-material>

References

- Abraham, M. J., Murtola, T., Schulz, R., Páll, S., Smith, J. C., Hess, B., et al. (2015). Gromacs: High performance molecular simulations through multi-level parallelism from laptops to supercomputers. *SoftwareX* 1, 19–25. doi:10.1016/j.softx.2015.06.001
- Allolio, C., Baxova, K., Vazdar, M., and Jungwirth, P. (2016). Guanidinium pairing facilitates membrane translocation. *J. Phys. Chem. B* 120, 143–153. doi:10.1021/acs.jpcc.5b10404
- Altrichter, S., Haase, M., Loh, B., Kuhn, A., and Leptihn, S. (2017). Mechanism of the spontaneous and directional membrane insertion of a 2-transmembrane ion channel. *ACS Chem. Biol.* 12, 380–388. doi:10.1021/acscchembio.6b01085
- Berger, O., Edholm, O., and Jähnig, F. (1997). Molecular dynamics simulations of a fluid bilayer of dipalmitoylphosphatidylcholine at full hydration, constant pressure, and constant temperature. *Biophys. J.* 72, 2002–2013. doi:10.1016/S0006-3495(97)78845-3
- Bjellmar, P., Larsson, P., Cuendet, M. A., Hess, B., and Lindahl, E. (2010). Implementation of the charmm force field in gromacs: Analysis of protein stability effects from correction maps, virtual interaction sites, and water models. *J. Chem. Theory Comput.* 6, 459–466. doi:10.1021/ct900549r
- Blazhynska, M., Goulard Coderc de Lacam, E., Chen, H., Roux, B., and Chipot, C. (2022). Hazardous shortcuts in standard binding free energy calculations. *J. Phys. Chem. Lett.* 13, 6250–6258. doi:10.1021/acs.jpclett.2c01490
- Bonhenry, D., Tarek, M., and Dehez, F. (2013). Effects of phospholipid composition on the transfer of a small cationic peptide across a model biological membrane. *J. Chem. Theory Comput.* 9, 5675–5684. doi:10.1021/ct400576e
- Bosshart, P. D., Jordanov, I., Garzon-Coral, C., Demange, P., Engel, A., Milon, A., et al. (2012). The transmembrane protein kpompa anchoring the outer membrane of klebsiella pneumoniae unfolds and refolds in response to tensile load. *Structure* 20, 121–127. doi:10.1016/j.str.2011.11.002
- Brambillasca, S., Yabal, M., Makarow, M., and Borgese, N. (2006). Unassisted translocation of large polypeptide domains across phospholipid bilayers. *J. Cell. Biol.* 175, 767–777. doi:10.1083/jcb.200608101
- Brambillasca, S., Yabal, M., Soffientini, P., Stefanovic, S., Makarow, M., Hegde, R. S., et al. (2005). Transmembrane topogenesis of a tail-anchored protein is modulated by membrane lipid composition. *EMBO J.* 24, 2533–2542. doi:10.1038/sj.emboj.7600730
- Broecker, J., Fiedler, S., Gimpl, K., and Keller, S. (2014). Polar interactions trump hydrophobicity in stabilizing the self-inserting membrane protein mistic. *J. Am. Chem. Soc.* 136, 13761–13768. doi:10.1021/ja5064795
- Chen, Y., Sotomayor, M., Capponi, S., Hariharan, B., Sahu, I. D., Haase, M., et al. (2022). A hydrophilic microenvironment in the substrate-translocating groove of the YidC membrane insertase is essential for enzyme function. *J. Biol. Chem.* 298, 101690. doi:10.1016/j.jbc.2022.101690
- Chin, C.-N., and von Heijne, G. (2000). Charge pair interactions in a model transmembrane helix in the er membrane. *J. Mol. Biol.* 303, 1–5. doi:10.1006/jmbi.2000.4122
- Cymer, F., Von Heijne, G., and White, S. H. (2015). Mechanisms of integral membrane protein insertion and folding. *J. Mol. Biol.* 427, 999–1022. doi:10.1016/j.jmb.2014.09.014
- Czajkowsky, D. M., Hotze, E. M., Shao, Z., and Tweten, R. K. (2004). Vertical collapse of a cytolysin prepore moves its transmembrane beta-hairpins to the membrane. *EMBO J.* 23, 3206–3215. doi:10.1038/sj.emboj.7600350
- Ding, J., Wang, K., Liu, W., She, Y., Sun, Q., Shi, J., et al. (2016). Pore-forming activity and structural autoinhibition of the gasdermin family. *Nature* 535, 111–116. doi:10.1038/nature18590
- Donald, J. E., Kulp, D. W., and DeGrado, W. F. (2011). Salt bridges: Geometrically specific, designable interactions. *Proteins* 79, 898–915. doi:10.1002/prot.22927
- Dorairaj, S., and Allen, T. W. (2007). On the thermodynamic stability of a charged arginine side chain in a transmembrane helix. *Proc. Natl. Acad. Sci. U. S. A.* 104, 4943–4948. doi:10.1073/pnas.0610470104
- Duart, G., Lamb, J., Ortiz-Mateu, J., Elofsson, A., and Mingarro, I. (2022). Intrahelical salt bridge contribution to membrane protein insertion. *J. Mol. Biol.* 434, 167467. doi:10.1016/j.jmb.2022.167467
- Gumbart, J., and Roux, B. (2012). Determination of membrane-insertion free energies by molecular dynamics simulations. *Biophys. J.* 102, 795–801. doi:10.1016/j.bpj.2012.01.021
- Huang, J., Rauscher, S., Nawrocki, G., Ran, T., Feig, M., De Groot, B. L., et al. (2017). Charrmm36m: An improved force field for folded and intrinsically disordered proteins. *Nat. Methods* 14, 71–73. doi:10.1038/nmeth.4067
- Johansson, A. C., and Lindahl, E. (2009). Titratable amino acid solvation in lipid membranes as a function of protonation state. *J. Phys. Chem. B* 113, 245–253. doi:10.1021/jp8048873
- Jorgensen, W. L., and Madura, J. D. (1985). Temperature and size dependence for Monte Carlo simulations of tip4p water. *Mol. Phys.* 56, 1381–1392. doi:10.1080/00268978500103111
- Kaminski, G. A., Friesner, R. A., Tirado-Rives, J., and Jorgensen, W. L. (2001). Evaluation and reparametrization of the opls-aa force field for proteins via comparison with accurate quantum chemical calculations on peptides. *J. Phys. Chem. B* 105, 6474–6487. doi:10.1021/jp003919d
- Klauda, J. B., Venable, R. M., Freites, J. A., O'Connor, J. W., Tobias, D. J., Mondragon-Ramirez, C., et al. (2010). Update of the charmm all-atom additive force field for lipids: Validation on six lipid types. *J. Phys. Chem. B* 114, 7830–7843. doi:10.1021/jp101759q
- Kovacs, S. B., and Miao, E. A. (2017). Gasdermins: Effectors of pyroptosis. *Trends Cell. Biol.* 27, 673–684. doi:10.1016/j.tcb.2017.05.005
- Laskowski, P. R., Pluhackova, K., Haase, M., Lang, B. M., Nagler, G., Kuhn, A., et al. (2021). Monitoring the binding and insertion of a single transmembrane protein by an insertase. *Nat. Commun.* 12, 7082. doi:10.1038/s41467-021-27315-3
- Lee, S., Channappanavar, R., and Kanneganti, T.-D. (2020). Coronaviruses: Innate immunity, inflammasome activation, inflammatory cell death, and cytokines. *Trends Immunol.* 41, 1083–1099. doi:10.1016/j.it.2020.10.005
- Lei, M., Gao, X., Yang, L., Yang, T., and Lian, X. (2011). Gsdma3 gene is needed for the induction of apoptosis-driven catagen during mouse hair follicle cycle. *Histochem. Cell. Biol.* 136, 335–343. doi:10.1007/s00418-011-0845-8
- Leung, C., Dudkina, N. V., Lukoyanova, N., Hodel, A. W., Farabella, I., Pandurangan, A. P., et al. (2014). Stepwise visualization of membrane pore formation by suliyisin, a bacterial cholesterol-dependent cytolysin. *eLife* 3, e04247. doi:10.7554/eLife.04247
- Li, J., Zhou, Y., Yang, T., Wang, N., Lian, X., and Yang, L. (2010). Gsdma3 is required for hair follicle differentiation in mice. *Biochem. Biophys. Res. Commun.* 403, 18–23. doi:10.1016/j.bbrc.2010.10.094
- Li, L., Vorobyov, I., and Allen, T. W. (2013). The different interactions of lysine and arginine side chains with lipid membranes. *J. Phys. Chem. B* 117, 11906–11920. doi:10.1021/jp405418y
- Liu, X., Xia, S., Zhang, Z., Wu, H., and Lieberman, J. (2021). Channelling inflammation: Gasdermins in physiology and disease. *Nat. Rev. Drug Discov.* 20, 384–405. doi:10.1038/s41573-021-00154-z

- Lluis, A., Schedel, M., Liu, J., Illi, S., Depner, M., von Mutius, E., et al. (2011). Asthma-associated polymorphisms in 17q21 influence cord blood ormdl3 and gsdma gene expression and il-17 secretion. *J. Allergy Clin. Immunol.* 127, 1587–1594. doi:10.1016/j.jaci.2011.03.015
- MacCallum, J. L., Bennett, W. D., and Tieleman, D. P. (2008). Distribution of amino acids in a lipid bilayer from computer simulations. *Biophys. J.* 94, 3393–3404. doi:10.1529/biophysj.107.112805
- MacCallum, J. L., Bennett, W., and Tieleman, D. P. (2007). Partitioning of amino acid side chains into lipid bilayers: Results from computer simulations and comparison to experiment. *J. Gen. Physiol.* 129, 371–377. doi:10.1085/jgp.200709745
- Mari, S. A., Pluhackova, K., Pipercevic, J., Leipner, M., Hiller, S., Engel, A., et al. (2022). Gasdermin-A3 pore formation propagates along variable pathways. *Nat. Commun.* 13, 2609. doi:10.1038/s41467-022-30232-8
- Mbaye, M. N., Hou, Q., Basu, S., Teheux, F., Pucci, F., and Rooman, M. (2019). A comprehensive computational study of amino acid interactions in membrane proteins. *Sci. Rep.* 9, 12043. doi:10.1038/s41598-019-48541-2
- Mishra, V., Palgunachari, M., Segrest, J., and Anantharamaiah, G. (1994). Interactions of synthetic peptide analogs of the class a amphipathic helix with lipids. evidence for the snorkel hypothesis. *J. Biol. Chem.* 269, 7185–7191. doi:10.1016/s0021-9258(17)37266-6
- Moon, C. P., and Fleming, K. G. (2011). Side-chain hydrophobicity scale derived from transmembrane protein folding into lipid bilayers. *Proc. Natl. Acad. Sci. U. S. A.* 108, 10174–10177. doi:10.1073/pnas.1103979108
- Mulvihill, E., Sborgi, L., Mari, S. A., Pfreundschuh, M., Hiller, S., and Müller, D. J. (2018). Mechanism of membrane pore formation by human gasdermin-d. *EMBO J.* 37, e98321. doi:10.15252/embj.201798321
- Mulvihill, E., van Pee, K., Mari, S. A., Müller, D. J., and Yildiz, Ö. (2015). Directly observing the lipid-dependent self-assembly and pore-forming mechanism of the cytolytic toxin listeriolysin o. *Nano Lett.* 15, 6965–6973. doi:10.1021/acs.nanolett.5b02963
- Oswald, J., Njenga, R., Natriashvili, A., Sarmah, P., and Koch, H.-G. (2021). The dynamic secyeg translocon. *Front. Mol. Biosci.* 8, 664241. doi:10.3389/fmolb.2021.664241
- Pluhackova, K., and Horner, A. (2021). Native-like membrane models of e. coli polar lipid extract shed light on the importance of lipid composition complexity. *BMC Biol.* 19, 4–22. doi:10.1186/s12915-020-00936-8
- Pluhackova, K., Wassenaar, T. A., and Böckmann, R. A. (2013). *Molecular dynamics simulations of membrane proteins*. Berlin, Germany: Springer.
- Pluhackova, K., Wassenaar, T. A., Kirsch, S., and Böckmann, R. A. (2015). Spontaneous adsorption of coiled-coil model peptides k and e to a mixed lipid bilayer. *J. Phys. Chem. B* 119, 4396–4408. doi:10.1021/acs.jpcc.5b00434
- Pluhařová, E., Marsalek, O., Schmidt, B., and Jungwirth, P. (2012). Peptide salt bridge stability: From gas phase via microhydration to bulk water simulations. *J. Chem. Phys.* 137, 185101. doi:10.1063/1.4765052
- Rizzo, R. C., and Jorgensen, W. L. (1999). Opls all-atom model for amines: Resolution of the amine hydration problem. *J. Am. Chem. Soc.* 121, 4827–4836. doi:10.1021/ja984106u
- Rogers, C., Erkes, D. A., Nardone, A., Aplin, A. E., Fernandes-Alnemri, T., and Alnemri, E. S. (2019). Gasdermin pores permeabilize mitochondria to augment caspase-3 activation during apoptosis and inflammasome activation. *Nat. Commun.* 10, 1689. doi:10.1038/s41467-019-09397-2
- Ruan, J., Xia, S., Liu, X., Lieberman, J., and Wu, H. (2018). Cryo-em structure of the gasdermin a3 membrane pore. *Nature* 557, 62–67. doi:10.1038/s41586-018-0058-6
- Runkel, F., Marquardt, A., Stoeger, C., Kochmann, E., Simon, D., Kohnke, B., et al. (2004). The dominant alopecia phenotypes bareskin, rex-denuded, and reduced coat 2 are caused by mutations in gasdermin 3. *Genomics* 84, 824–835. doi:10.1016/j.ygeno.2004.07.003
- Saeki, N., Usui, T., Aoyagi, K., Kim, D. H., Sato, M., Mabuchi, T., et al. (2009). Distinctive expression and function of four gsdm family genes (gsdma-d) in normal and malignant upper gastrointestinal epithelium. *Genes Chromosom. Cancer* 48, 261–271. doi:10.1002/gcc.20636
- Sandoval-Perez, A., Pluhackova, K., and Böckmann, R. A. (2017). Critical comparison of biomembrane force fields: Protein–lipid interactions at the membrane interface. *J. Chem. Theory Comput.* 13, 2310–2321. doi:10.1021/acs.jctc.7b00001
- Schaefer, S. L., and Hummer, G. (2022). Sublytic gasdermin-D pores captured in atomistic molecular simulations. *bioRxiv*. doi:10.1101/2022.06.02.494496
- Shi, J., Gao, W., and Shao, F. (2017). Pyroptosis: Gasdermin-mediated programmed necrotic cell death. *Trends biochem. Sci.* 42, 245–254. doi:10.1016/j.tibs.2016.10.004
- Shi, J., Zhao, Y., Wang, K., Shi, X., Wang, Y., Huang, H., et al. (2015). Cleavage of gsdmd by inflammatory caspases determines pyroptotic cell death. *Nature* 526, 660–665. doi:10.1038/nature15514
- Söderman, J., Berglund, L., and Almer, S. (2015). Gene expression-genotype analysis implicates gsdma, gsdmb, and lrcc3c as contributors to inflammatory bowel disease susceptibility. *Biomed. Res. Int.* 2015, 834805. doi:10.1155/2015/834805
- Souza, P., Alessandri, R., Barnoud, J. e. a., Thallmair, S., Faustino, I., Grunewald, F., et al. (2021). Martini 3: A general purpose force field for coarse-grained molecular dynamics. *Nat. Methods* 18, 382–388. doi:10.1038/s41592-021-01098-3
- Strandberg, E., and Killian, J. A. (2003). Snorkeling of lysine side chains in transmembrane helices: How easy can it get? *FEBS Lett.* 544, 69–73. doi:10.1016/s0014-5793(03)00475-7
- Terao, C., Kawaguchi, T., Dieude, P., Varga, J., Kuwana, M., Hudson, M., et al. (2017). Transethnic meta-analysis identifies gsdma and prdm1 as susceptibility genes to systemic sclerosis. *Ann. Rheum. Dis.* 76, 1150–1158. doi:10.1136/annrheumdis-2016-210645
- Ulmschneider, J. P. (2017). Charged antimicrobial peptides can translocate across membranes without forming channel-like pores. *Biophys. J.* 113, 73–81. doi:10.1016/j.bpj.2017.04.056
- Ulmschneider, M. B., Ulmschneider, J. P., Schiller, N., Wallace, B. A., Von Heijne, G., and White, S. H. (2014). Spontaneous transmembrane helix insertion thermodynamically mimics translocon-guided insertion. *Nat. Commun.* 5, 4863. doi:10.1038/ncomms5863
- van Dalen, A., and de Kruijff, B. (2004). The role of lipids in membrane insertion and translocation of bacterial proteins. *Biochim. Biophys. Acta* 1694, 97–109. doi:10.1016/j.bbamcr.2004.03.007
- van Pee, K., Mulvihill, E., Müller, D. J., and Yildiz, Ö. (2016). Unraveling the pore-forming steps of pneumolysin from streptococcus pneumoniae. *Nano Lett.* 16, 7915–7924. doi:10.1021/acs.nanolett.6b04219
- Vazdar, M., Heyda, J., Mason, P. E., Tesei, G., Allolio, C., Lund, M., et al. (2018). Arginine "magic": Guanidinium like-charge ion pairing from aqueous salts to cell penetrating peptides. *Acc. Chem. Res.* 51, 1455–1464. doi:10.1021/acs.accounts.8b00098
- Vögele, M., Bhaskara, R. M., Mulvihill, E., van Pee, K., Yildiz, Ö., Kühlbrandt, W., et al. (2019). Membrane perforation by the pore-forming toxin pneumolysin. *Proc. Natl. Acad. Sci. U. S. A.* 116, 13352–13357. doi:10.1073/pnas.1904304116
- Walle, L. V., and Lamkanfi, M. (2016). Pyroptosis. *Curr. Biol.* 26, R568–R572. doi:10.1016/j.cub.2016.02.019
- Wang, Q., Wang, Y., Ding, J., Wang, C., Zhou, X., Gao, W., et al. (2020). A bioorthogonal system reveals antitumour immune function of pyroptosis. *Nature* 579, 421–426. doi:10.1038/s41586-020-2079-1
- Wang, Y., Hu, D., and Wei, D. (2014). Transmembrane permeation mechanism of charged methyl guanidine. *J. Chem. Theory Comput.* 10, 1717–1726. doi:10.1021/ct400738r
- Wassenaar, T. A., Pluhackova, K., Böckmann, R. A., Marrink, S. J., and Tieleman, D. P. (2014). Going backward: A flexible geometric approach to reverse transformation from coarse grained to atomistic models. *J. Chem. Theory Comput.* 10, 676–690. doi:10.1021/ct400617g
- Webb, B., and Sali, A. (2016). Comparative protein structure modeling using modeller. *Curr. Protoc. Bioinforma.* 54, 5.6.1–5.6.37. doi:10.1002/cpbi.3
- Wimley, W. C. (2002). Toward genomic identification of β -barrel membrane proteins: Composition and architecture of known structures. *Protein Sci.* 11, 301–312. doi:10.1110/ps.29402
- Xia, S., Zhang, Z., Magupalli, V. G., Pablo, J. L., Dong, Y., Vora, S. M., et al. (2021). Gasdermin d pore structure reveals preferential release of mature interleukin-1. *Nature* 593, 607–611. doi:10.1038/s41586-021-03478-3
- Yang, A., Gunner, M., Sampogna, R., Sharp, K., and Honig, B. (1993). On the calculation of pKs in proteins. *Proteins* 15, 252–265. doi:10.1002/prot.340150304
- Yu, J., Kang, M.-J., Kim, B.-J., Kwon, J.-W., Song, Y.-H., Choi, W.-A., et al. (2011). Polymorphisms in gsdma and gsdmb are associated with asthma susceptibility, atopy and bhr. *Pediatr. Pulmonol.* 46, 701–708. doi:10.1002/ppul.21424
- Zahid, A., Ismail, H., and Jin, T. (2021). Molecular and structural aspects of gasdermin family pores and insights into gasdermin-elicited programmed cell death. *Biochem. Soc. Trans.* 49, 2697–2710. doi:10.1042/BST20210672
- Zheng, M., Williams, E. P., Malireddi, R. S., Karki, R., Banoth, B., Burton, A., et al. (2020). Impaired nlrp3 inflammasome activation/pyroptosis leads to robust inflammatory cell death via caspase-8/ripk3 during coronavirus infection. *J. Biol. Chem.* 295, 14040–14052. doi:10.1074/jbc.RA120.015036